Model-based attenuation of movement artifacts in fMRI

T. Lemmin [a,b,1], G. Ganesh [b,c,*,1], R. Gassert [d,a], E. Burdet [c], M. Kawato [b], M. Haruno [b]

[a] *Ecole Polytechnique Fédérale de Lausanne (EPFL), Switzerland*
[b] *Computational Neuroscience Laboratories, ATR International, Japan*
[c] *Department of Bioengineering, Imperial College London, United Kingdom*
[d] *Department of Mechanical and Process Engineering, ETH Zurich, Switzerland*

ARTICLE INFO

ABSTRACT

Behavioral analysis of multi-joint arm reaching has allowed important advances in understanding the control of voluntary movements. Complementing this analysis with functional magnetic resonance imaging (fMRI) would give insight into the neural mechanisms behind this control. However, fMRI is very sensitive to artifacts created by head motion and magnetic field deformation caused by the moving limbs. It is thus necessary to attenuate these motion artifacts in order to obtain correct activation patterns. Most algorithms in literature were designed for slow changes of head position over several brain scans and are not very effective on data when the movement is of duration below the resolution of a brain scan. This paper introduces a simple model-based method to remove motion artifacts during short duration movements. The proposed algorithm can account for head movement and field deformations due to movements within and outside of the scanner's field of view. It uses information from the experimental design and subject kinematics to focus the artifact attenuation in time and space and minimize the loss of uncorrupted data. Applications of the algorithm on arm reaching experimental data obtained with blocked and event-related designs demonstrate attenuation of motion artifacts with minimal effect on the brain activations.

© 2010 Elsevier B.V. All rights reserved.

1. Introduction

The study of multi-joint arm reaching has been the mainstay of upper-body motor control research for over a century (Woodworth, 1899), and allowed important advances in human motor control (e.g. Abend et al., 1982; Mussa-Ivaldi et al., 1985; Shadmehr and Mussa-Ivaldi, 1994; Gomi and Kawato, 1996; Burdet et al., 2001; Franklin et al., 2008). On the other hand, speech studies investigating physiological and acoustic phonetics rely on movement characterization of speech organs like the tongue, lips, jaw, velum and the vocal folds (Kent, 1997). Studies in both these fields, involving short discrete movements, have relied on the analysis of kinematics and muscle activity to infer control of these tasks.

Complementing these data with functional magnetic resonance imaging (fMRI) could give important insights into the neural mechanisms involved in human motor control and related dysfunctions (Diedrichsen et al., 2005; Tunik et al., 2007). Specialized robotic interfaces (Gassert et al., 2006a, 2006b) and EMG collection (Ganesh et al., 2007a) have recently been developed, which allow us to perform a diverse range of motor control experiments during fMRI.

However, these experiments invariably involve limb movements, and fMRI is very sensitive to head movements and magnetic field changes that may occur due to moving body limbs (Birn et al., 2004). Both head and body movements can lead to motion artifacts inducing false-positive activity or masking real brain activation. Furthermore, major brain regions involved in motor control are located on the cortex, which is at the boundary of the brain and the skull. Motion artifacts, which typically appear at contrast edges (Birn et al., 2004), are thus likely to affect the investigation of motor control significantly. Therefore, in order to determine correct functional activation maps during motor tasks, it becomes crucial to attenuate these motion artifacts.

Processing of images with rigid body image realignment is the most common technique used for online (Steger and Jackson, 2004; Thesen et al., 2000) and offline (Bursztyn et al., 2006; Steger and Jackson, 2004; Kim et al., 1999; Friston et al., 1996) attenuation of movement artifacts. Other methods proposed in literature use optical tracking (Dold et al., 2006, 2005), navigator pulses (Ward et al., 2000; Lee et al., 1996) or offline analysis of signal variance (Huang et al., 2008; Diedrichsen and Shadmehr, 2005; Hickok, 2003) to estimate head movement and attenuate the artifacts, with online slice corrections (Ward et al., 2000; Lee et al., 1996), downweighting of corrupted images (Diedrichsen and Shadmehr, 2005) or replacing

---

* Corresponding author at: Computational Neuroscience Labs, ATR International, 2-2-2, Hikaridai, Seika-cho, Soraku-gun, 6190288 Kyoto, Japan.
Tel.: +81 774 95 1230; fax: +81 774 95 1236.
E-mail addresses: gganesh@atr.jp, gans_gs@hotmail.com (G. Ganesh).
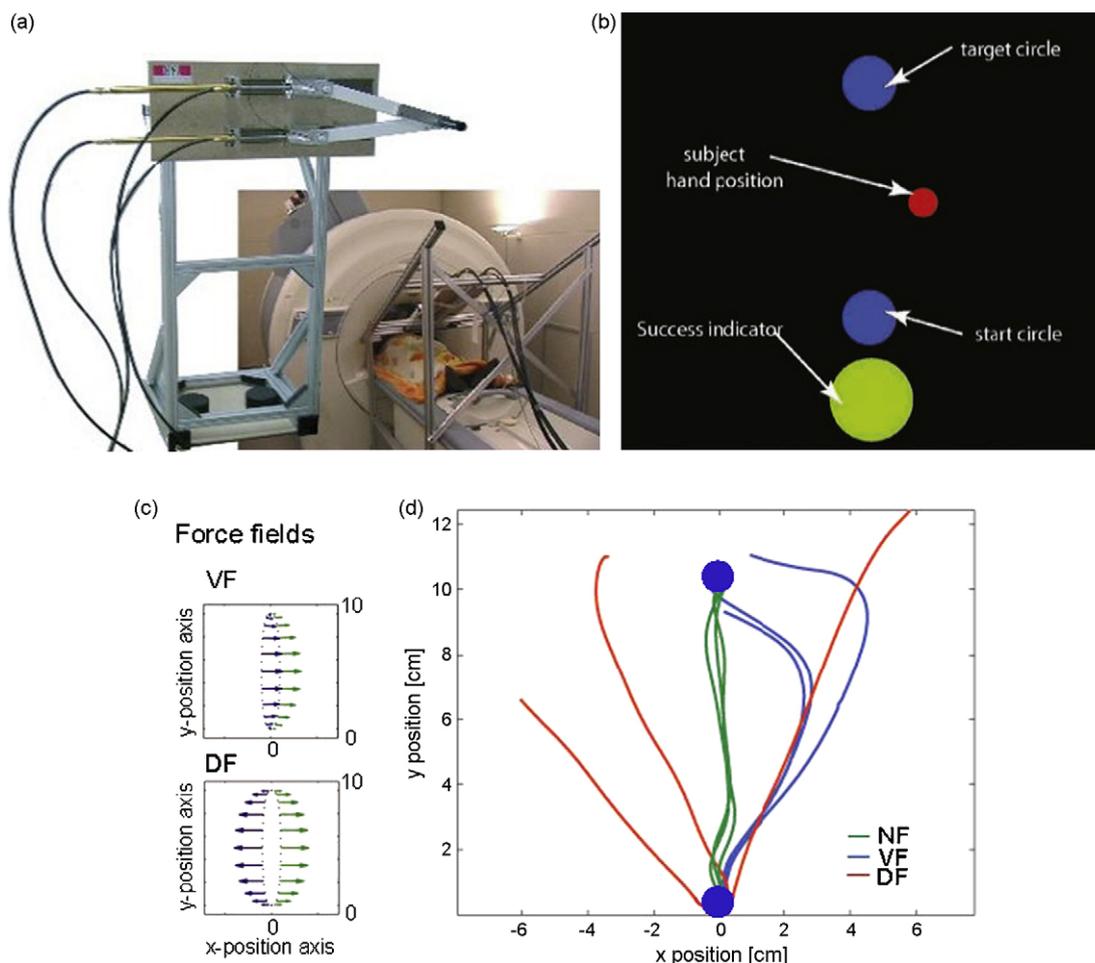
Fig. 1. (a) A 2 degree-of-freedom MR-compatible interface produces computer-controlled interaction with arm movements. The subject lies in a supine position while the interface, supported on an aluminum frame, is placed in front of the scanner. The subject can reach the manipulandum handle and move it in a plane at an angle to the bed. (b) The subject receives visual feedback of the start and end target positions (blue disks) and of the current hand position (red disk). Success or failure of the movement is indicated by a green or red light at the bottom of the screen. (c) Three representative force field were considered: a null force field (NF), a velocity-dependent force field (VF) and a position-dependent divergent force field (DF). (d) The effect of these force fields on forward movements.

artifact-affected values by interpolation (Huang et al., 2008). However, all these methods estimate parameters only every repetition time (TR) (which has a resolution of a few seconds) and are insensitive to short-duration movements as involved in arm reaching and speech, which typically last less than a second. Higher resolution methods recently proposed (Speck et al., 2006; Zaitsev et al., 2006) become difficult to use during motor experiments, especially arm reaching, where a manipulandum, visual feedback screen and their support structures impede optical tracking.

Although little is known about the artifacts created by arm movements, results from speech experiments show that head movement and magnetic field deformations due to body movements (Birn et al., 2004) are the major contributors to motion artifacts. A brain scan consists of a collection of small scanned volumes called voxels defined by a coordinate frame fixed to the scanner. Head movement and magnetic field deformations due to change in limb positions cause a shift between the scanner and head coordinates leading to a shift of voxels relative to the head. This may result in voxels moving into a region with different signal intensity, either due to material or functional differences, causing a sudden change in the signal value and resulting in an artifact. These motion artifacts thus tend to be concentrated at contrast edges in the brain (Birn et al., 2004) where small shifts can induce large signal changes due to the varying material properties.

While head movement artifacts affect voxels directly due to their movement, magnetic field deformation artifacts can be caused even when the head does not move but there is movement of other limbs in the neighborhood. The large amount of artifacts seen in the simple contrast between two conditions when the subject relaxed in two different arm postures gives a quantitative estimate of magnetic field deformation induced by the change in limb position (Fig. 6).

In addition, the shift of a voxel into a region of different field intensity leads to a change in saturation of spin magnetization which can create 'spin history artifacts' (Muresan et al., 2005; Friston et al., 1996), the practical considerations for correction of which have been explored in Robson et al. (1997). Here we will not consider changes in the fMRI signal due to the spin history, as a TR of 3.5 s is long enough such that this effect becomes small (Grootoonk et al., 2000).

The brain response as detected by fMRI is commonly modeled using the haemodynamic response function (hrf) corresponding to the local variation of relative levels of oxy-haemoglobin and deoxy-haemoglobin due to an impulse stimulation. In its canonical shape, this response peaks approximately five seconds after the stimulus. As the motion artifacts considered here are induced directly by the movement of tissue, they occur within a short time period immediately after movement onset (Birn et al., 2004). Thus, for short and discrete reaching movements commonly examined in
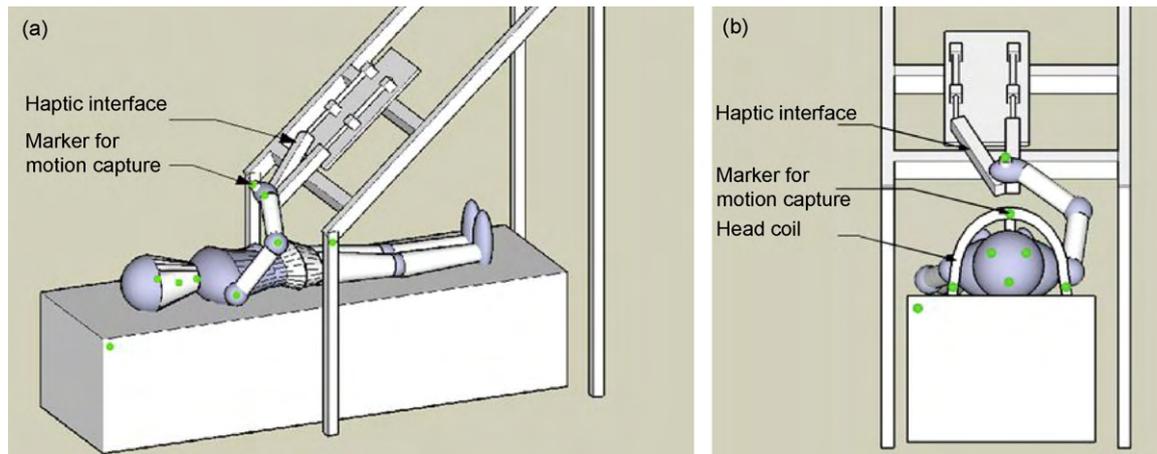
Fig. 2. Position of markers used for motion capture. Markers were fixed (a) on the shoulder, arm and robot and (b) on the head of each subject.

motor control (e.g. Shadmehr and Mussa-Ivaldi, 1994; Burdet et al., 2001), artifacts have a different time course than the detected brain activity.

The model-based method presented in this paper utilizes this temporal activity difference to distinguish artifacts due to head movement and field deformations from actual brain activity, followed by a spatio-temporally localized smoothing procedure to attenuate them. Evaluation of the effect of the algorithm on artifacts resulting from reaching movements made in different dynamic environments demonstrate that the algorithm can attenuate artifacts in both event-related and blocked fMRI experiments, without affecting real brain activity. The attenuation algorithm was implemented as Matlab functions that can be easily integrated into SPM5 (download from http://www.cns.atr.jp/~gganesh/motion_correction.zip).

2. Methods

Movement artifacts were evaluated for planar multi-joint arm movements. Seven human subjects without known neuropathology (right-handed males aged between 23 and 40 years) performed point-to-point reaching movements in force fields produced by a robotic interface (Fig. 1a, Gassert et al., 2006b), first outside the MR room, while arm, shoulder and head movements were recorded using motion capture, and then inside the scanner, during fMRI. The institutional ethics committee at ATR approved the experiments and participating subjects gave informed consent before participation.

The recorded subject movements were first used to create a spatio-temporal model of the head and shoulder movements. This model was then used to localize the movement artifacts spatially and temporally, followed by artifact attenuation. The various steps of the procedure are explained in the following sections.

2.1. Reaching task

Subjects lay in a supine position, while holding the handle of an MR-compatible arm interface (Gassert et al., 2006b) and made 10 cm long point-to-point reaching movements from a start circle defined at coordinates (0,0) cm to a target at coordinates (0,10) cm displayed on the screen visible to the subject (Fig. 1b). A cursor indicated the current hand position during the movement. The movement start was cued by two short audio beeps, each 100 ms in duration and with an interval of 200 ms, followed by a long beep lasting 650 ms corresponding to the movement time. Once the movement was completed, the hand was brought back to the start by the robot after a specified *wait time.* The wait time was kept as

either 1 s or varied between 5 and 7 s to realize two different types of fMRI experiment designs, 'blocked' and 'event-related' respectively. The subjects were instructed to relax during this return movement. A movement was considered as successful if the subject reached the target in 650 ± 50 ms and stopped his hand inside the target circle. To inform the subject on the success or failure of a trial, a large green or red circle was displayed at the bottom of the screen (Fig. 1b) during the passive return. Note that while the random wait time in the event-related design helps desynchronize the imaging and movement, in the blocked design, de-synchronization is achieved by avoiding imaging repetition time (TR) being a multiple of the total movement cycle time (=300 ms beep + 650 ms movement + 1 s wait time + 1 s return = ~3 s).

Reaching movements were performed in three representative force fields:

1. A null field (NF) in which no force field is applied by the manipulandum's actuators, i.e. the subject only experiences the apparent dynamics of the manipulandum.
2. A position-dependent divergent force field (DF) producing an additional force perpendicular to the straight line from the start to the target and proportional to the distance from this line:

$$\begin{bmatrix} F_x \\ F_y \end{bmatrix} = \begin{bmatrix} 300x \\ 0 \end{bmatrix}, \tag{1}$$

where the force is in N, and x in m (see Fig. 1c).
3. A velocity-dependent force field (VF) defined by:

$$\begin{bmatrix} F_x \\ F_y \end{bmatrix} = \begin{bmatrix} 0 & 13 \\ -13 & 0 \end{bmatrix} \begin{bmatrix} \dot{x} \\ \dot{y} \end{bmatrix} \tag{2}$$

where the velocities $\dot{x}$, $\dot{y}$ are in m/s.

Typical trajectories in these force fields recorded by the MR-compatible 2 degree-of-freedom (2DOF) interface are shown in Fig. 1d.

2.2. Experiments

2.2.1. Experiment 1: quantification of head and shoulder movement

Motion capture was performed at 100 Hz using an NDI Optotrak 3020 system to measure arm and head movements while the subject performed the reaching task. The movements were quantified in the experimental position on the scanner bed, with the head coil and bite bar in place but with the scanner bed moved out from the scanner bore.
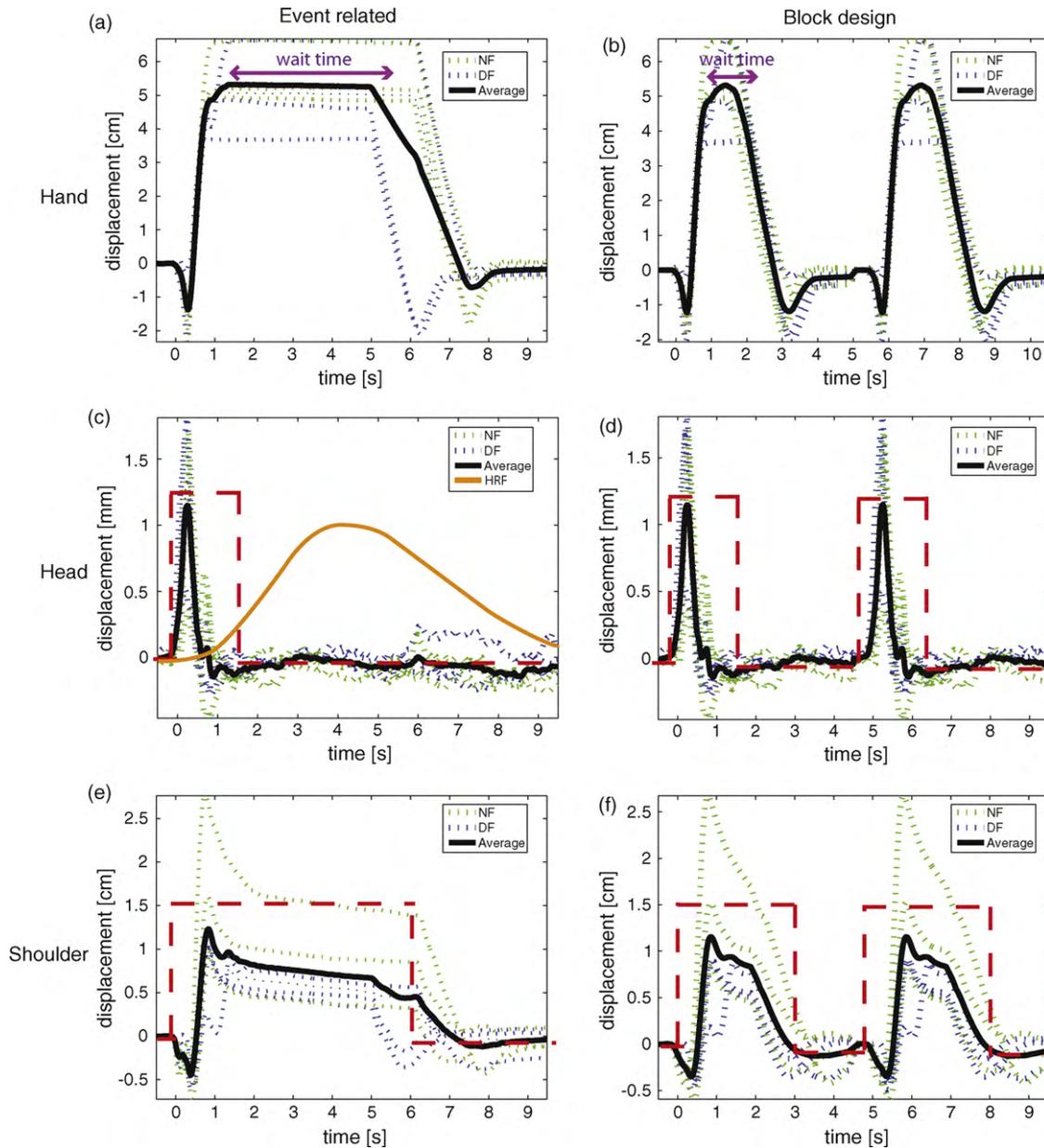
Fig. 3. Movement profiles during reaching. The movement of hand (a and b), head (c and d) and shoulder (e and f) during event (left column) and blocked (right column) experiments are shown for different force fields. The hand movement closely matches the shoulder movement both in the event and blocked designs. The head movement profile is similar in both event (c) and blocked (d) designs and occurs in the first 1.5 s when the hand is moving. The shoulder movement (e and f) forms a plateau equal in length to the wait time of the experiment. The movement profiles may be fitted by boxcar functions (red dashed traces). For the head movements, the width of the boxcar corresponds to the period after the start of movement till when the movement is below 10% of the maximum displacement. For the shoulder movement, the boxcar width corresponds to the wait time. In comparison, the orange trace of (c) shows the expected hemodynamic response function (as modeled by SPM).

Four markers were placed on the shoulder, elbow, and wrist articulations, as well as on the robotic interface, as shown in Fig. 2. Three additional markers were fixed on the subject's head in order to evaluate rotation and translation during movement by considering a six degree-of-freedom (DOF) rigid body model. In addition, three markers on the coil allowed examining for any movements of the coil, and one marker on the bed served as the reference for the measurements.

The absolute displacement of the head and shoulder was calculated as ($\sqrt{\Delta x^2 + \Delta y^2 + \Delta z^2}$), where the terms represent the change in voxel position in the x, y and z coordinates respectively in the image. The temporal evolution of the displacement is plotted for each force field in (Fig. 3).

2.2.2. Experiment 2: imaging study

For the fMRI experiments, a 1.5 T MR scanner (Shimadzu-Marconi ECLIPSE 1.5T Power Drive 250) was used to obtain blood oxygen level dependent (BOLD) contrast functional images. Images weighted with the apparent transverse relaxation time were obtained with a gradient-echo echo-planar imaging (EPI) sequence. Data were collected at a repetition time (TR) of 3.5 s with echo time 50 ms; flip angle 90°, 35 slices (of thickness 3.5 mm and gap 1 mm) of 64 × 64 in plane voxels (in-plane field of view of 224 mm^2) covering the entire brain.

The subjects made 105 movements in a blocked design and 52 movements in an event-related design experiment. The scans recorded from these movements were treated

Table 1
Summary of the experiments.

Experiment	Aim	Remarks
1	Movement quantification	7 subjects Movements measured using optical tracking of arm, shoulder and head 26 movements in event-related design
2	Imaging study for evaluation of artifact attenuation	7 subjects 105 movements made in blocked design 52 movements made in the event-related design fMR images obtained treated with attenuation algorithm to evaluate the algorithm
3	Artifacts from shoulder movement	3 subjects, 2 right handed and 1 left handed Subject's hand moved and maintained at the two ends of the reaching movement repetitively for 40 s each Contrast of fMR images during the two conditions analyzed for artifacts
4	Checking for false positives	7 subjects Subjects pressed a button with their finger (instead of making a reaching movement) in a blocked design paradigm fMR images were analyzed with and without application of the attenuation algorithm to check for false positives/negatives

with the artifact attenuation algorithm to test the algorithm.

2.2.3. Experiment 3: artifacts from shoulder movement

To elucidate artifacts due to shoulder movement, a subsidiary experiment was carried out with three subjects (two right handed and one left handed). The subject's hand was fixed onto the MR-compatible manipulandum while they had to relax in a supine position in the scanner. The manipulandum moved the subject's hand repetitively between two positions corresponding to the start and target positions of the reaching task. At each position the hand was maintained for 40 s. A standard SPM contrast analysis was performed between the conditions when the hand was at the two different positions. As the subjects relaxed during the whole measurement, and each position was maintained for a long period (40 s), a contrast is expected to give activity related to just the change in shoulder/arm position.

2.2.4. Experiment 4: checking for false positives

Verification that the algorithm does not remove brain activity or add false-positive activity can be achieved by observing the effects of the algorithm in the absence of artifacts. This was done with a button press experiment, in which movement artifacts are expected to be minimal, as the movements involved are small and far from the head coil.

The seven subjects were presented with the same visual and audio cues as in the reaching experiment. The subjects held the interface with their left hand and rested the fingers of their right hand on MR-compatible push buttons[2] placed on the scanner bed at the height of their hips. On receiving the cue to move, the subjects were asked to press the buttons under their index and middle fingers for the duration of the movement time. We verified that there was minimal movement of the head, arm and interface during this experiment, thus no movement artifacts are expected in the results. The images from this experiment were then analyzed with and without the artifact attenuation algorithm to see how it modifies the activity map (Table 1).

2.3. Algorithm

2.3.1. Modeling motion artifacts

If we consider a voxel located at the boundary of two contrast regions corresponding to different materials (e.g. brain tissue and bone) or functional properties, head movement and magnetic field deformation may shift this voxel into the neighboring region, thus changing the signal intensity and leading to movement artifacts. As the artifacts are an immediate consequence of the movement, the temporal pattern of this movement can be directly used to model the artifact.

It was seen in Section 2.2 that the amplitude of head movement was close to the spatial resolution of the imaging sequence used. In addition, head and shoulder displacements had a similar time profile independent of the force field (Fig. 3). Thus, we assume that each reaching movement produces comparable effects on the imaging. To model the head movement, the displacement profiles were aligned to the movement onset as detected by the manipulandum, and averaged over trials. The average peaks before the first second of movement (Fig. 3c and d) and then decreases slowly back to the baseline. We determined the time point (after this peak) after which the absolute value of displacement remains below 10% of the peak, which was found to occur around 1.5 s from movement start in all subjects. We thus model the head movement by a simple boxcar function with 1.5 s duration starting at the onset of the reaching movement. The shoulder displacement is modeled by a boxcar function of the length of the *wait period* (Fig. 3e and f).

2.3.2. Spatial localization of artifact

The brain response as detected by fMRI is commonly modeled using the haemodynamic response function (hrf) as a basis function (Amaro and Barker, 2006). The hrf corresponds to the local variation of oxy-haemoglobin due to an impulse stimulation and in its canonical shape, this response peaks approximately 5 s after the stimulus onset (Fig. 3c). Each stimulus during an experiment can be modeled as an impulse function locked at the onset of the cue. The brain activation regressor is estimated by convolving its basis function with this impulse series[3]:

$$\mathbf{X} = \mathbf{hrf}^T[\mathbf{x_1}, \mathbf{x_2}, \dots, \mathbf{x_m}], \tag{3}$$

---

[2] Bimanual 4 (Model No: HH-2x2), fiber optic response pad, Current Designs Inc., Philadelphia.

[3] By convention, scalars s are italic, column vectors v are bold and matrices M are capitalized bold.
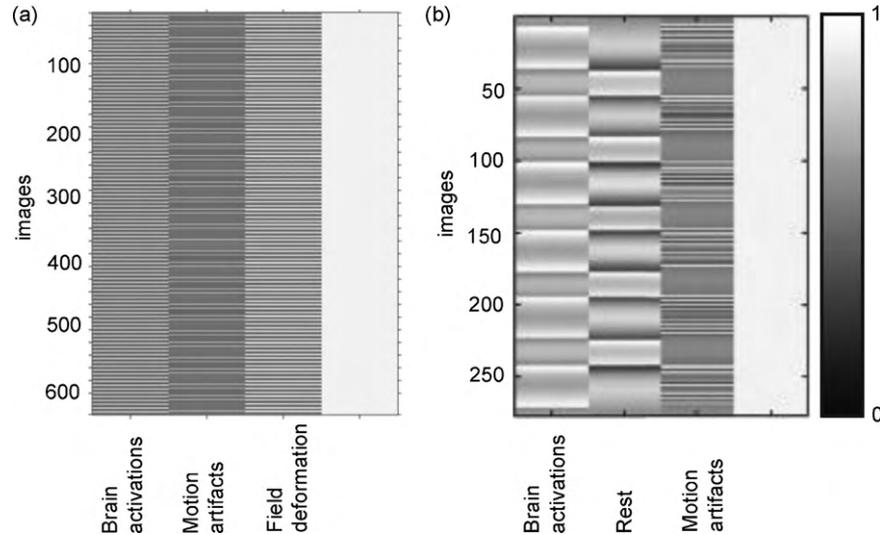
Fig. 4. Design matrices for noise detection. The experiment matrix consisted of four columns (regressors). (a) For the event-related experiment, brain activity (events convolved with the hrf) forms the first column, head movement artifact (events convolved with head mbf) forms the second column, field deformation artifact (events convolved with shoulder mbf) forms the third column and fourth column accounts for the base line. (b) For the blocked design matrix, the first and second column form the active and rest conditions. Motion artifacts (movement time convolved with mbf) forms the third column and accounts for both head movement and field deformations.

where **hrf** is the hrf time series vector, $\mathbf{x_1}$ represents the reaching movement event, and $\mathbf{x_2}, \ldots, \mathbf{x_m}$ are $m-1$ impulse trains, each corresponding to a regressor for one of the other events under observation. All $\mathbf{x_i}$ are column vectors with n time points. Assuming that the total brain activation in a voxel is the sum of the contributions from each regressor, the brain voxels corresponding to each regressor are estimated by the respective regression parameter β which corresponds to the least-square fit, i.e. minimizing

$$\left\|\mathbf{Y} - \mathbf{X}\beta\right\|^2, \tag{4}$$

where $\mathbf{Y}$ represents the $n \times k$ array of brain activity time series of k voxels, and β the $m \times k$ matrix of regression parameters.

To detect the artifact-contaminated voxels in the fMRI images, an additional regressor Z is formed, which represents the movement artifacts. The artifacts are aligned with the movements and can be represented in time by a simple boxcar function as was described in Section 2.3. We use a corresponding motion basis function (mbf) (Fig. 3b) and define Z as the convolution of the mbf with the reaching movement event $\mathbf{x_1}$:

$$\mathbf{Z} = \mathbf{mbf}^T\left[\mathbf{x_1}\right], \tag{5}$$

where **mbf** is the mbf time series vector. The voxel time series becomes a combination of brain activation and motion artifacts. We can estimate the voxels affected by the movement artifacts by extending Eq. (4) and minimizing:

$$\left\|\mathbf{Y} - \begin{bmatrix} \mathbf{X} & \mathbf{Z} \end{bmatrix} \begin{bmatrix} \beta \\ \gamma \end{bmatrix}\right\|^2. \tag{6}$$

The corresponding SPM design matrix is shown in Fig. 4a. Note that as the shoulder and head regressors were similar in the blocked design (Fig. 3d and f), SPM did not allow for two separate mbfs but a single mbf corresponding to the head movement could be used to isolate both the head and shoulder artifacts. For the event-related case, a separate mbf is added for detecting the shoulder artifacts (Fig. 4b).

The parameters β and γ significantly different from zero, correlated with the brain activation and motion artifact regressors, can then be isolated by using a Fisher's statistical test (F-test) to detect increasing or decreasing activity related to the mbf. While the F-test gives us a statistical map, the threshold used on this map is

critical to correctly identify motion artifacts. A high threshold will detect only part of the artifact-affected voxels, neglecting voxels with relatively low artifacts, and setting the threshold too low may lead to false positives where voxels may be wrongly assumed to contain artifacts. The following automated procedure is proposed to estimate a suitable threshold using SPM5:

1. A conservative threshold of $p < 0.001$ uncorrected is used on the F-test in order to obtain the activation maps corresponding to the hrf (i.e. to brain activity) and to the mbf (artifacts).
2. The hrf map is masked (inclusively) with the mbf map, yielding a statistical map of the mbf voxels which also significantly contribute to hrf activity (i.e have significantly high β). In this map, the coordinates of the voxel with minimum p-value would correspond to the mbf voxel which has the most significant contribution to hrf activity, and thus relatively, the least contribution to mbf activity. The coordinates of the voxel with the minimum p-value are noted and, referring back to the mbf activation map, the p-value of the same voxel in this map is then used as the threshold for the mbf activation map.

2.3.3. Temporal localization of artifacts

During fMRI using echo-planar imaging (EPI), brain activity is measured one two-dimensional slice at a time, every slice acquisition time. All these slices are combined every repetition time (TR) to form a complete three-dimensional image. The slice acquisition time for the 1.5 T scanner used in this study is about 100 ms. As the head movement lasts for only 1.5 s after every movement onset, only the slices acquired during this period are potentially affected by motion artifacts. In the last step we isolated the voxels in the images affected by artifacts. It is important to note that these voxels are generally not contaminated throughout the entire time series, but artifacts are present only when the slices containing these voxels were scanned immediately after the movement. Using the known timing of the movements and slice acquisition order, we can identify the specific data points in the time series of each of the affected voxels, which can contain movement artifacts. Isolating artifacts temporally makes it possible to treat only the affected data points. In contrast, a general attenuation algorithm may also attenuate activity corresponding to real brain activation. Detecting slices that may be affected by artifacts is particularly useful in
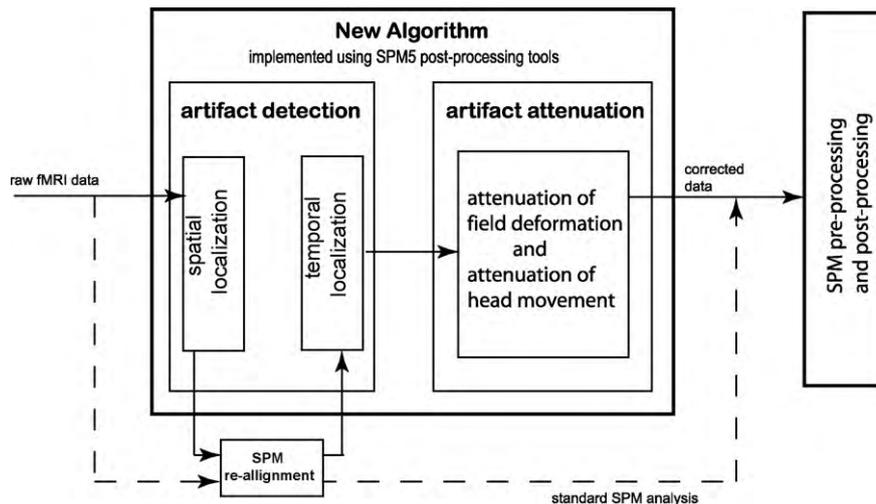
Fig. 5. Steps of the artifact attenuation algorithm described in Section 2.

event-related designs, where the artifact and actual brain activity lead to similarly high peaks in the voxel time series, and may therefore be difficult to distinguish using general dynamic features.

2.3.4. Attenuation of artifacts in blocked design

In the blocked design experiment the movements occur roughly every 5–6 s. The voxel data, on the other hand, can be acquired in a relatively shorter time period corresponding to the TR for a whole brain scan. This represents 2–5 s with a 1.5 T scanner and can be even shorter with a stronger magnet or for partial brain scans. Thus it is reasonable to assume that, in the voxel time series, the data collected before or after an artifact-contaminated value are free from head movement artifacts (which are modeled by a 1.5 s boxcar function). Therefore, to attenuate the artifact, spatially and temporally localized artifact-affected voxels are replaced by the linear interpolation of the data values of the previous and following temporal neighbors. If $V_k(n)$ represents the value of the k-th voxel in space, and n-th data point in time, which may be affected by motion, then the corrected value for this point, $V_k^c(k)$, is computed as

$$V_k^c(k) = \frac{V_k(n-1) + V_k(n+1)}{2}. \tag{7}$$

This simple estimator, assuming that the brain activity changes slowly, was found to work well in blocked design for both head and shoulder movement artifacts.

2.3.5. Attenuation of artifacts in event-related design

In the case of a blocked design with movements in quick succession, the head and shoulder/arm movement regressors are not significantly different, and both the head movement and magnetic field deformation artifacts may be isolated by a single mbf. In the case of event-related designs, two mbfs were added during the detection phase, one corresponding to the head, similar to the blocked design, and one to the arm/shoulder movements to detect the related magnetic field deformations separately. As the deformation artifacts last for a longer period and more than one TR, they are attenuated by a slightly different procedure from the head artifacts, as

$$V_k^c(n) = V_k(n) - \left(\overline{V_k(e)} - \overline{V_k} \right), \tag{8}$$

where e represents the indices of all immediate temporal neighbors recorded during the *wait period* and $\overline{V_k(e)}$ represents the mean activity during this period. $\overline{V_k}$ represents the mean activity in the voxel. The basis of this correction is that the boxcar model used to isolate the shoulder artifact assumes 'noisy' voxels to have a

slightly different baseline than the average for that voxel. Thus in Eq. (8) we average the voxel activity during the wait period to get the noisy baseline $\left(\overline{V_k(e)} \right)$, and find the difference of this baseline from the voxel average and hence the noise $\left(\overline{V_k(e)} - \overline{V_k} \right)$. This value is subtracted from each of the noisy value to remove the noise.

2.4. Implementation in SPM5

The described attenuation algorithm can in principle be implemented using any software package computing linear modeling of activity in the brain. The results presented in this paper yield from an implementation as Matlab functions integrated within the SPM5[4] graphical user interface (GUI). Realignment in SPM extracts the six rigid body model parameters controlling translation and rotation of the head along the three principal axes during the movement. These parameters can be used to form supplementary regressors during the analysis.

As the realignment parameters are calculated every TR, but the short movement affects only a few slices, realignment leads to an averaging effect. The artifacts are removed partially while some errors are spread into the other slices (Freire and Mangin, 2001). As the proposed algorithm treats the artifacts slice-wise, it seems logical to apply the artifact detection (Section 2.5) algorithm before the realignment process. However, considering the fact that our algorithm is insensitive to slow drifts, which are captured better by the realignment procedure, realigning the images can reduce errors in our attenuation procedure (Sections 2.7 and 2.8). The following procedure is thus followed in SPM:

1. After the first few scans of the experiment are discarded to allow for magnetic equilibration, the raw, non-realigned images are then analyzed with a design matrix consisting of the expected brain activity **X** (Eq. (3)) and the expected movement related activity **Z** (Eq. (5)). In case of a blocked design, an additional regressor may be added for the rest condition. Our implementation allows for an easy configuration of the required mbf and parallel analysis with two different basis functions (Fig. 4).
2. The obtained activation maps corresponding to brain activity and movement artifact are then thresholded to spatially localize the artifacts as described in this section.
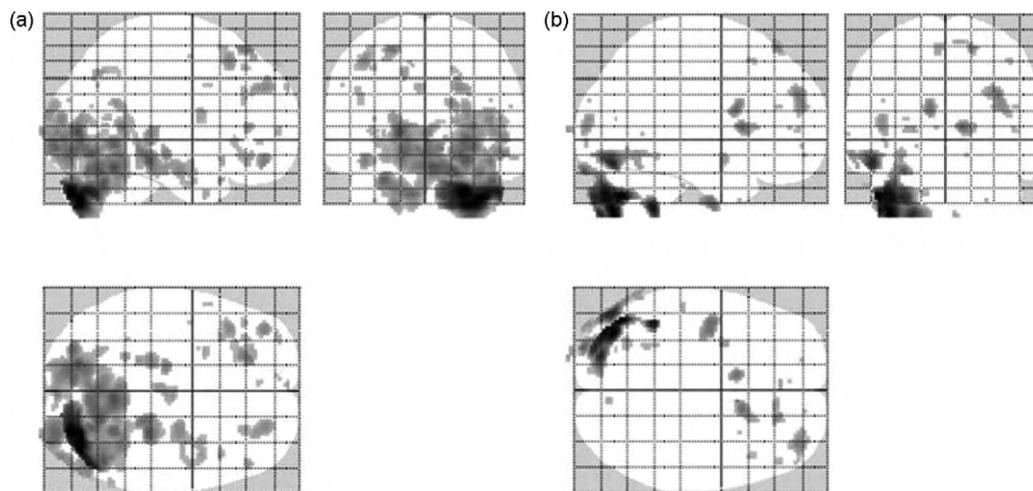
Fig. 6. Magnetic field deformation. (a) For right-handed subjects the field deformation artifacts were found to be concentrated in the right cerebellum and lower occipital lobe, both of which are close to the moving shoulder and arm ($p < 0.001$ uncorrected). (b) For a left-handed subject, the mirror image of the pattern was found where the left areas of the brain were affected, corresponding to the movement of the subject's left limb ($p < 0.001$ uncorrected).

3. The images are then realigned in SPM and the same realignment transformations applied to the detected artifact voxels as well.
4. This is followed by the temporal localization (Section 2.5) and attenuation realized as described in Sections 2.6 and 2.7.
5. The artifact-attenuated data can now be treated as realigned raw data from the experiment and analyzed following the regular steps of pre-processing (un-warping, co-registration, normalization and smoothing) and post processing with the regular experimental regressors, including the SPM5 generated movement regressors.

The block diagram of Fig. 5 summarizes the algorithm and its steps.

3. Results

3.1. Shoulder movement (field deformation) artifacts

The results of the contrast analysis from two individuals, (A) one right handed and one (B) left handed, from experiment 3 are shown in Fig. 6. Note that the cerebellum and lower visual regions close to the shoulder of the moving arm show significant (t-test, $p < 0.001$, uncorrected) differences between conditions where only the hand position changed (corresponding to field deformation artifacts). The difference in head position was insignificant (paired t-test, $p < 0.001$) between the two conditions.

3.2. Spatial localization of artifacts

Fig. 7 shows the voxels isolated by the head movement mbf in the blocked (Fig. 7a) and head (Fig. 7b) and shoulder (Fig. 7c) movement mbfs in the event-related designs for a representative subject during reaching movements in representative force fields. A high concentration of activity is observed along the tissue boundaries of the cortex and ventricles. This is in agreement with the expected location of the motion artifacts (Section 1). A similar effect was observed in all subjects.

3.3. Temporal localization of artifacts

The spatially localized artifacts were isolated in time before being attenuated. The example time series of an artifact-affected voxel from the motor cortex, before and after correction (Fig. 8b)

shows that only some selected time points, which were time localized as artifact affected, were treated by the algorithm. These correspond to the slices which were images within the mbf (1.5 s) of the movement onset.

3.4. Head artifact attenuation and evaluation

In order to evaluate the attenuation capabilities of the algorithm, we analyzed data from each subject, with and without applying the attenuation algorithm before the SPM processing. Data from a representative subject are shown in Fig. 9 while the multi-subject analysis is shown in Fig. 10.

In the primary motor region, application of our algorithm led to an insignificant decrease in the number of voxels ($p = 0.84$, Fig. 10b) in all the subjects. While it is generally difficult to distinguish artifact from brain activity, the activity inside ventricles can be classified with certainty as artifact, and we thus analyzed how well our algorithm can remove this activity. The number of significant voxels ($p < 0.001$, uncorrected) was compared before and after attenuation (Fig. 10a).

Among the subjects, there was a mean decrease of 64% of voxels in the ventricles after application of our algorithm ($p < 0.001$). In comparison, application of the Robust Weighted Least Squares (RWLS) algorithm (Diedrichsen et al., 2005), where each image is weighted with the inverse of its variance, showed no significant change in the number of voxels ($p = 0.12$ and $p = 0.14$ respectively) before and after attenuation.

Fig. 11 shows multi-subject fixed effect model of the activity detected for the button press of Experiment 4, (A) with versus (B) without the artifact attenuation algorithm. Significant activity ($p < 0.001$ uncorrected) is observed in the left motor cortex, in agreement with previous studies on finger tapping (Hanakawa et al., 2006) and also in parts of the cingulate and visual cortex. Importantly, application of the attenuation algorithm on the same data does not add or remove any activity in the images ($p < 0.05$), and the coordinates of the peak activity centers remain unchanged. This demonstrates that the attenuation algorithm does not add any false positives or false negatives in the images.

3.5. Field deformation artifact attenuation

Analysis of the event-related experiment with the mbf corresponding to shoulder movement isolated the regions close
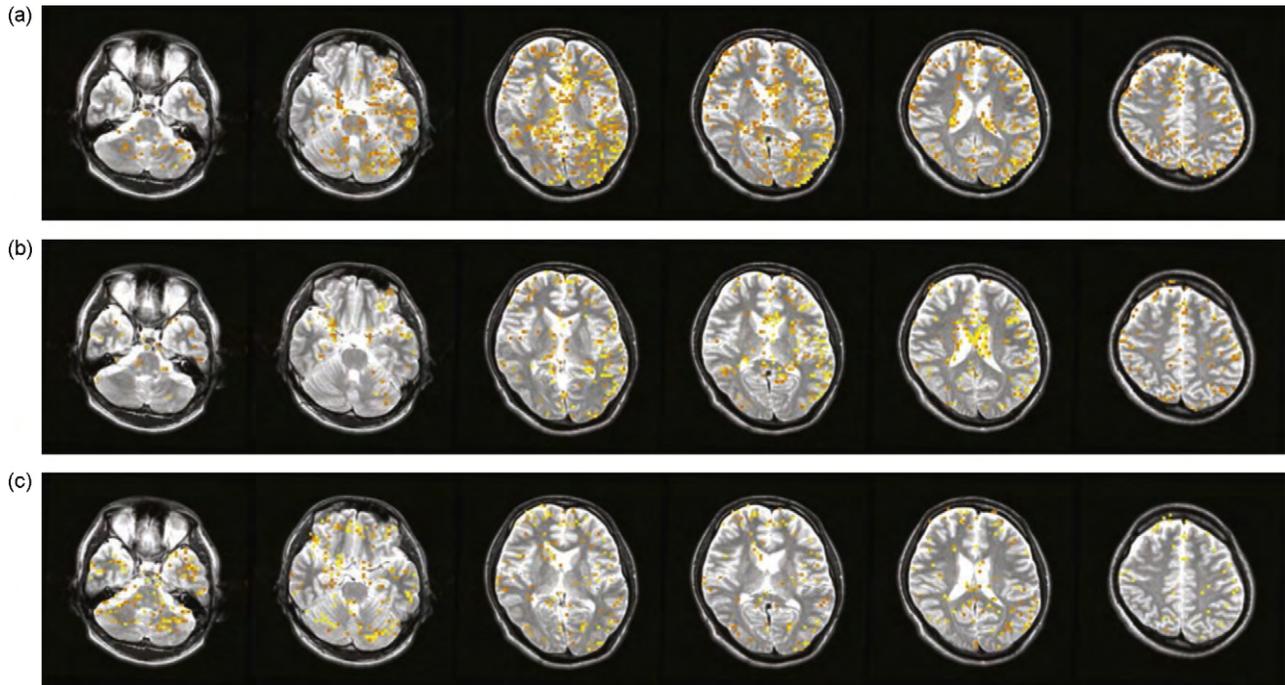
Fig. 7. Artifact localization in space. The figure shows artifacts detected in slices from the brain image of the same subject in blocked (a) and event-related (b and c) experiments. While a single mbf detects both the head and field deformation artifacts in the blocked design (a), the head (b) and field deformation (c) were isolated by separate mbfs in the event-related experiment. The figure shows statistical maps from a representative subject ($p < 0.001$ uncorrected).
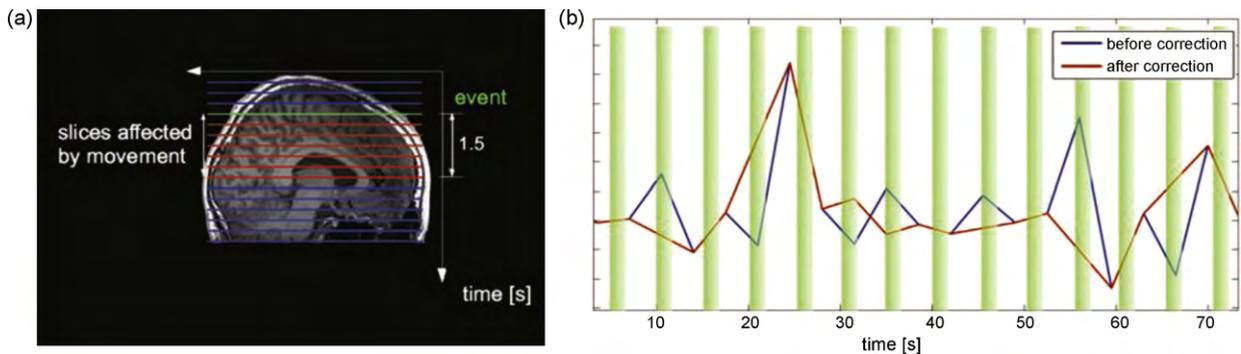
Fig. 8. Selective attenuation of data points in time. (a) The brain is scanned one 2-dimensional slice at a time during echo-planar imaging (EPI). As the head movement artifacts occur only in the first 1.5 s after a movement, only a few specific slices (red) are affected by it, which can be used localize the particular data points in time that may be affected. Though in this figure the slices are shown to be scanned serially to ease explanation, scanning during longer TR is often done through interleaved acquisition, which is accounted for in the algorithm. (b) The figure shows a part of the time series of a voxel before (blue) and after (red) attenuation. Due to the attenuation of artifacts in specific slices, only the few peaks occurring immediately after a movement are attenuated while others are not attenuated. The non-attenuated data points occur outside the green region in the figure where artifacts can be expected.
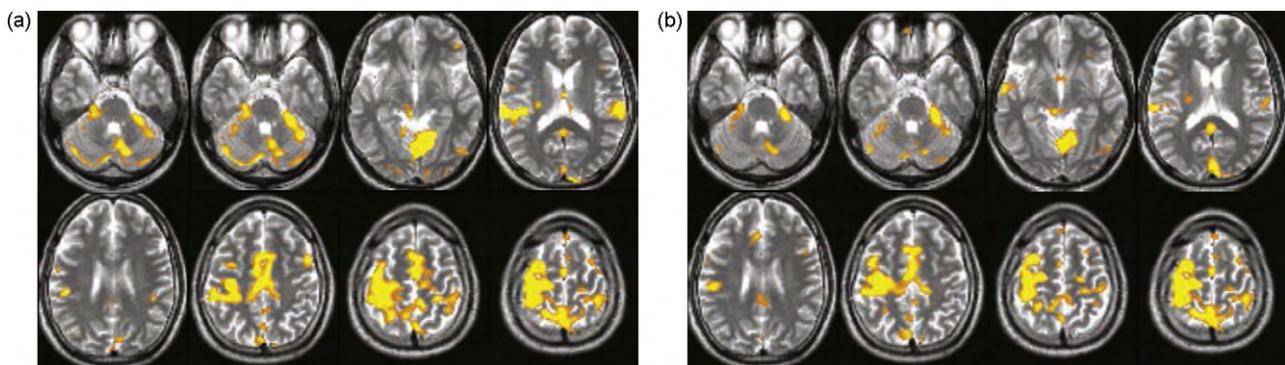
Fig. 9. Artifact cleaned images. Superimposition (a) on the structural slices from a representative subject shows the activity corresponding to the motor event without the application of the artifact attenuation algorithm. When the algorithm was applied and the same analytical procedure was repeated, significant removal of activity from boundaries can be seen in the selected slices (b) ($p < 0.05$ uncorrected), especially from the boundaries of the cerebellum and parts of the motor cortex.
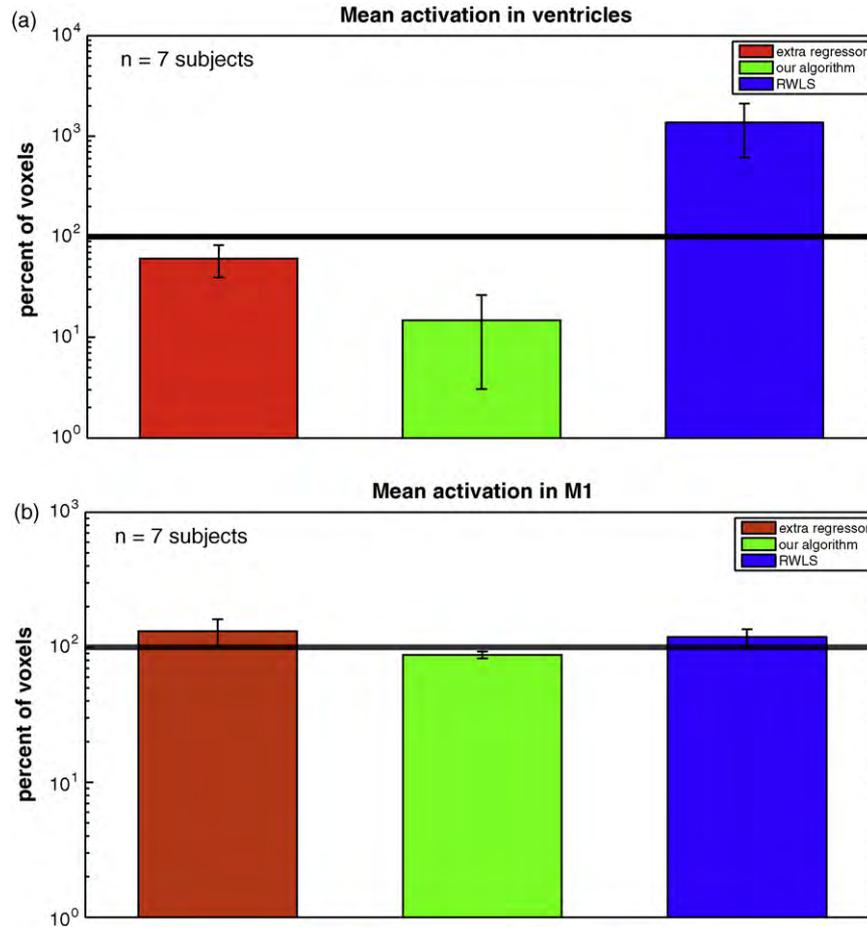
Fig. 10. The percentage of voxels ($p < 0.001$, uncorrected) inside the ventricles (a) and in left M1 (b) with respect to conventional SPM analysis for blocked design. Three attenuation algorithms were tested: adding the mbf as an extra regressor to the conventional SPM analysis (red), our attenuation algorithm (green) and RWLS as proposed in Diedrichsen et al. (2005) (blue). Pseudo-activation in ventricles is significantly reduced with our algorithm ($p < 0.0003$) but not with the extra regressor or RWLS method ($p = 0.12$ and $p = 0.14$ respectively). Whereas the activations in M1 remain similar to the conventional analysis with all algorithms ($p < 0.05$, $p < 0.33$ and $p < 0.29$, respectively). The error bars indicate standard error.

to the moving arm/shoulder (as shown in the glass brain of Fig. 12a and slices of Fig. 12b). These regions are similar to Fig. 6a and b. Upon application of the attenuation procedure, the field deformation artifacts were visibly reduced (Fig. 12b). Both figures are plotted at a threshold of $p < 0.001$, uncorrected.

4. Discussion

Motor control experiments during fMRI require movement of limbs and invariably lead to head movement, inducing artifacts in the functional brain images. This paper introduced a model-based method to attenuate these artifacts and obtain a useful
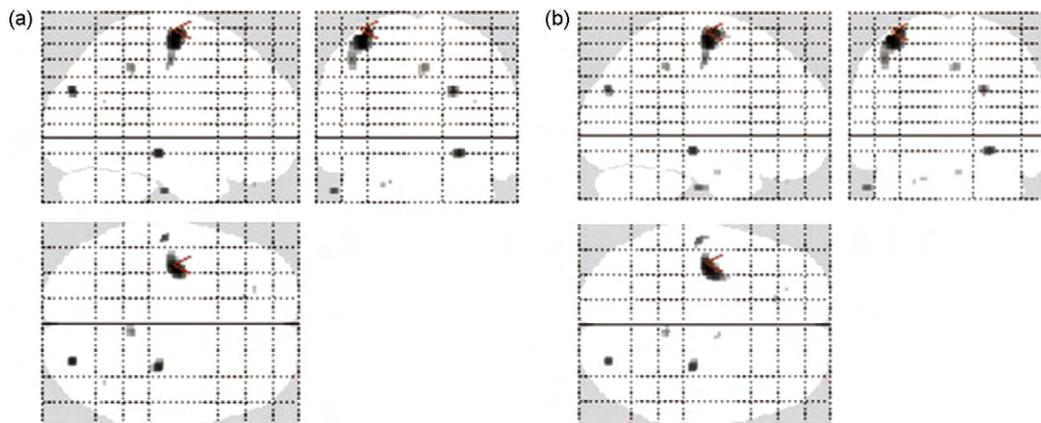
Fig. 11. The proposed algorithm does not attenuate brain activity. A button press study (which is expected to have minimal movement artifacts) was analyzed using the standard SPM procedure, with (a) and without (b) the application of our attenuation algorithm. The event-related contrast of finger tapping gave no significant activity ($p < 0.001$ uncorrected) between the two images for seven subjects. This confirms that brain activity was not affected by the artifact attenuation process. The figure shows the glass brain of a representative subject.
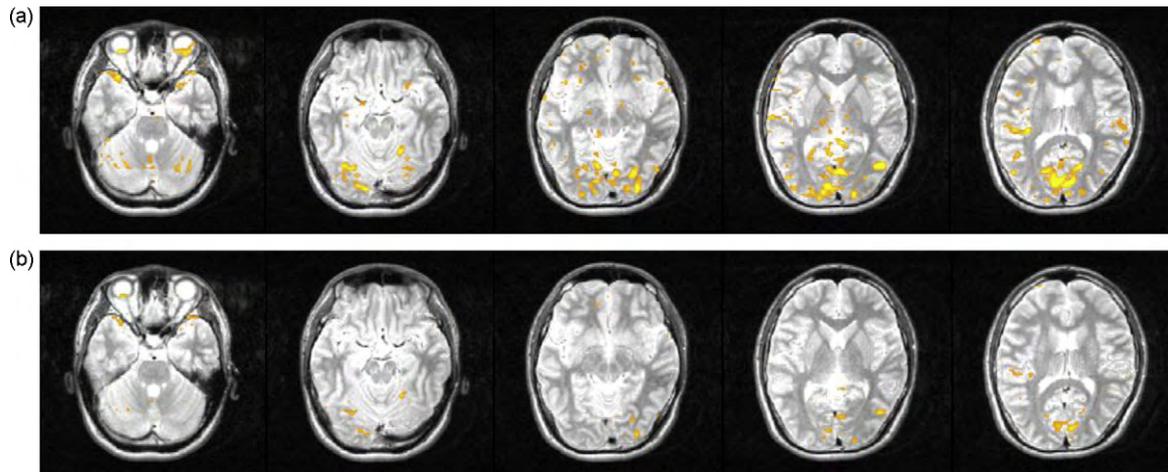
Fig. 12. Correction for magnetic field deformation. In the event-related design, the mbf corresponding to shoulder/arm movements (for the same right-handed subject as Fig. 6a) isolates artifacts localized in the right cerebellum and lower right occipital lobe, very similar to the regions seen in Fig. 6a. Some slices from the superposition on the structure image are shown in (a). After correction, the field deformation artifacts were significantly reduced in (b). The figure shows the statistical map of a representative subject ($p < 0.001$ uncorrected).

functional map. Voxels deteriorated by artifacts were detected by linear regression with a motion basis function (mbf) approximating the head movement, and their intensity was corrected only over the time period in which it could have been affected. The experimental results demonstrated that this method efficiently attenuates motion artifacts both in event-related and blocked designs, without introducing false-positive brain activity.

The proposed model-based method is fundamentally different from statistical methods proposed in the literature (Diedrichsen and Shadmehr, 2005; Huang et al., 2008), which detect significant changes in signal magnitude to identify artifacts, or rigid body movements (Friston et al., 1996). These methods are designed to work for relatively slow movements and hence correct at the resolution of a TR, while their performance deteriorates when the movement is short and discrete (Fig. 10). In contrast, the proposed method was designed specifically for short duration movements like arm reaching and speech. Using all available information on movement time, duration and repeatability, the model-based method is able to localize the artifact in time and space, thus minimizing loss of data not related to artifacts, which is a major concern with the statistical methods of Diedrichsen and Shadmehr (2005) and Huang et al. (2008). However, the proposed algorithm cannot handle artifacts due to slow movements. Therefore, if both short and long duration movements are expected, our algorithm may be used in series with other algorithms. For example, in this paper our algorithm was used in series with SPM realignment (Friston et al., 1996) to remove any signal drift that cannot be handled by our algorithm.

An important aspect of the artifact detection is the choice of the artifact model (mbf). While the average of the recorded movement forms the best model for the detection, we aimed to simplify this model so as to negate the requirement of a quantification experiment (motion recording) every time the algorithm is used. Several empirical models (including a triangle, boxcar of varying width and step with an exponential decay) were tried as candidate models to fit the movement profile of the head (Fig. 3c and d). Among these, the boxcar model with a width equal to the time period of head movement (1.5 s) performed similar to an mbf corresponding to the average movement profile. Our model aims to capture two aspects of the artifacts: temporal (the time period at which artifacts occur) and magnitude (the signal pattern that is followed). As the fMRI signal is noisy, it is likely that the temporal information (time of occurrence) becomes more important for detection than the sig-

nal value, which would explain why the temporal information is captured well by the simple boxcar design. The boxcar regressor requires only the event duration which can be inferred from the interface (e.g. position) sensors, and does not require motion capture, so is the most practical mbf.

The second important consideration to enable good artifact detection (and hence attenuation) is in the experiment design. For event-related designs the wait period should ideally be fixed over 10 s so as to: (i) isolate the head and shoulder movement separately with different mbfs, and (ii) keep the shoulder mbf different from the hrf. However, the long 'wait period' of course makes the experiment time longer and other tasks may require temporally close movement repetitions (like the blocked design example we considered). Even for blocked designs, if not correlated, then separate regressors are preferred for the head and field deformation artifacts. The correlation of regressors is reported automatically by SPM during regressor definition, and may be also checked manually using singular value decomposition of the regressors.

At the same time, a blocked design experiment normally shows higher signal to noise ratio in fMRI studies. This is due to the fact that (i) more trials are possible in a shorter time, and (ii) it is easier to detect a general change in the baseline activity than the actual activity profile as in an event-related case. For movement artifact detection as well in blocked design, the hrf activity is almost constant at a high value due to the closeness of the movements in time. On the other hand, the movement artifact related 'activity' peaks only during the movement phases. It is thus much easier (with higher statistical significance) to isolate the artifact in this case rather than in the event-related case where both artifact and hrf activity are changing with time. Furthermore, irrespective of the design and like in any other fMRI analysis, artifact detection achieves higher statistical significance if there are more trials. Especially in the event analysis, it is thus encouraged to use as many trials as possible (in respect to other constraints).

A major problem for all artifact attenuation methods is to distinguish artifact activity from actual brain activity. While activity aligned along tissue boundaries and inside ventricles may be classified with some certainty as artifacts, it is difficult to distinguish artifact from actual brain activity in the interior of the brain. As both artifact and brain activity vary between subjects, a multi-subject analysis does not help in this regard. We thus chose to analyze the performance of our algorithm by its performance in the ventricles (Fig. 10), assuming that a good performance in the ventricles would

indicate an appreciable performance in the interior of the brain as well. Furthermore, the button press experiment (Fig. 11a and b) demonstrated that the algorithm does not add any artifacts in the images nor does it affect brain activity.

The boxcar function used to model the artifacts due to the head displacement or the magnetic field deformation assumes that the voxels move into a region with a different material or functional property, and return back to the original position when the movement is completed. When using a bite bar, the head movement during reaching was shown to be small and satisfy this assumption. However, in the case of field deformation, the apparent movement of the voxels may be larger. Therefore, some voxels may move to a region with similar material and functional properties as the region they actually belong to, thus inducing a different time profile of activity than assumed by our model.

In order to detect motion artifacts efficiently, it is important to estimate the movement start accurately. The audio or visual cue provided to the subject during an experiment can be used to estimate movement onsets. However, such cues will not capture reaction delays and movement duration, which may vary significantly between trials, nor will they allow detection of missed trials. Therefore, if the experiment involves a robotic device interacting with the limbs as in our case, movement information from the device's sensors should be used to extract these parameters.

Though the algorithm was demonstrated here on discrete reaching movements, it can also be applied to attenuate the artifacts from other kinds of short duration movements. While we provide the simple mbf that works well for reaching movements, speech and other motor studies may require suitable mbfs corresponding to the specific limb movement involved. These should be evaluated using optical measurements, as suggested in Section 2.2. Note that, as the limb movement model is a function of time and does not depend on space, the algorithm can be used for movements irrespective of their spatial properties. The performance will, however, depend on how different the mbf, which models the artifact activity, is from the hrf, which models brain activity. This is usually not a concern during discrete reaching movements, which typically last less than one second, but may have a non-negligible effect for slower movements. Consideration of these timing issues during the design of the experiment can help extract the best possible performance from the artifact attenuation algorithm.

Acknowledgements

Appendix A. Supplementary data

Supplementary data associated with this article can be found, in the online version, at doi:10.1016/j.jneumeth.2010.07.013.

References

Abend W, Bizzi E, Morasso P. Human trajectory formation. Brain 1982; 105(2):331–48.

Amaro E, Barker GJ. Study design in fMRI: basic principles. Brain Cogn 2006; 60(3):220–32.

Birn R, Cox R, Bandettini P. Experimental designs and processing strategies for fMRI studies involving overt verbal responses. NeuroImage 2004;23:1046–58.

Burdet E, Osu R, Franklin DW, Milner TE, Kawato M. The central nervous system stabilizes unstable dynamics by learning optimal impedance. Nature 2001;414:446–9.

Bursztyn L, Ganesh G, Imamizu H, Kawato M, Flanagan R. Neural correlates of internal-model loading. Curr Biol 2006;16:2440–5.

Diedrichsen J, Shadmehr R. Detecting and adjusting for artifacts in fMRI time series data. NeuroImage 2005;27(3):624–34.

Diedrichsen J, Hashambhoy Y, Rane T, Shadmehr R. Neural correlates of reach errors. J Neurosci 2005;25(43):9919–31.

Dold C, Zaitsev M, Speck O, Firle EA, Hennig J, Sakas G. Prospective head motion compensation for MRI by updating the gradients and radio frequency during data acquisition. Proc Int Conf Med Image Comput Comput Assist Interv 2005;8(1):482–9.

Dold C, Zaitsev M, Speck O, Firle EA, Hennig J, Sakas G. Advantages and limitations of prospective head motion compensation for MRI using an optical motion tracking device. Acad Radiol 2006;13(9):1093–103.

Franklin DW, Burdet E, Tee KP, Osu R, Chew CM, Milner TE, et al. CNS learns stable, accurate, and efficient movements using a simple algorithm. J Neurosci 2008;28(44):11165–73.

Freire L, Mangin JF. Motion correction algorithms may create spurious brain activations in the absence of subject motion. NeuroImage 2001;14(3):709–22.

Friston K, Williams S, Howard R, Frackowiak R, Turner R. Movement-related effects in fMRI time-series. Magn Reson Med 1996;35:346–55.

Ganesh G, Franklin DW, Gassert R, Imamizu H, Kawato M. Accurate real-time feedback of surface EMG during fMRI. J Neurophysiol 2007a;97(1):912–20.

Gassert R, Moser R, Burdet E, Bleuler H. An MRI/fMRI compatible robotic system with force-feedback for interaction with human motion. IEEE/ASME Trans Mech 2006a;11(2):216–24.

Gassert R, Dovat L, Lambercy O, Ruffieux Y, Chapuis D, Ganesh G, et al. A 2-DOF fMRI compatible haptic interface to interact with arm movements. In: Proc. IEEE international conference on robotics and automation (ICRA); 2006b. p. 3825–31.

Gomi H, Kawato M. Equilibrium-point control hypothesis examined by measured arm stiffness during multi-joint movement. Science 1996;272:117–20.

Grootoonk S, Hutton C, Ashburner J, Howseman AM, Rees JO, Friston KJ, et al. Characterization and correction of interpolation effects in the realignment of fMRI time series. NeuroImage 2000;11:49–57.

Hanakawa T, Honda M, Zito G, Dimyan MA, Hallett M. Brain activity during visuo-motor behavior triggered by arbitrary and spatially constrained cues: an fMRI study in humans. Exp Brain Res 2006;172(2):275–82.

Hickok G. Functional brain imaging. In: MIT encyclopedia of communication disorders; 2003.

Huang J, Francis C, Carr TH. Studying overt word reading and speech production with event-related fMRI: a method for detecting, assessing and correction articulation induces signal changes and for measuring onset time and duration of articulation. Brain Language 2008;104(1):10–23.

Kent R. The speech sciences. San Diego: Singular Publishing Group, Inc; 1997.

Kim B, Boes JL, Bland PH, Chenevert TL, Meyer CR. Motion correction in fMRI via registration of individual slices into an anatomical volume. Magn Reson Med 1999;41:964–72.

Lee CC, Grimm RC, Manduca A, Felmlee JP, Ehman RL, Riederer SJ, et al. A prospective approach to correct for inter-image head rotation in fMRI. MRM 1996;39:234–43.

Muresan L, Renken R, Roerdink J, Duifhuis H. Automated correction of spin-history related motion artefacts in fMRI: simulated and phantom data. IEEE Trans Biomed Eng 2005;52:1450–60.

Mussa-Ivaldi FA, Hogan N, Bizzi E. Neural, mechanical and geometric factors subserving arm postures in humans. J Neurosci 1985;5(10):2732–43.

Robson MD, Gatenby JC, Anderson AW, Gore JC. Practical considerations when correcting for movement-related effects present in fMRI time-series. In: Proc. ISMRM 5th annual meeting; 1997. p. 1681.

Shadmehr R, Mussa-Ivaldi FA. Adaptive representation of dynamics during learning of a motor task. J Neurosci 1994;14:3208–24.

Speck O, Hennig J, Zaitsev M. Prospective real-time slice-by-slice motion correction for fMRI in freely moving subjects. MAGMA 2006;19(2):55–61.

Steger TR, Jackson EF. Real-time motion detection of functional fMRI data. J Appl Clin Med Phys 2004;5(2):64–70.

Thesen S, Heid O, Schad LR. Prospective acquisition correction for head motion with image-based tracking for real-time fMRI. Magn Reson Med 2000;44:457–65.

Tunik E, Schmitt PJ, Grafton ST. BOLD coherence reveals segregated functional neural interactions when adapting to distinct torque perturbations. J Neurophysiol 2007;97(3):2107–20.

Ward HA, Riederer SJ, Grimm RC, Ehman RL, Felmlee JP, Clifford RJ. Prospective multiaxial motion correction for fMRI. Magn Reson Med 2000;43:459–69.

Woodworth RS. The accuracy of voluntary movement. Psychol Rev 1899;3:1–119.

Zaitsev M, Dold C, Sakas G, Hennig J, Speck O. Magnetic resonance imaging of freely moving objects: prospective real-time motion correction using an external optical motion tracking system. NeuroImage 2006;31(3):1038–50.